JOURNAL OF GEOPHYSICAL RESEARCH, VOL. 112, D07105, doi:10.1029/2006JD007245, 2007

Assessment of interannual variations in the surface mass balance of 18 Svalbard glaciers from the Moderate Resolution Imaging Spectroradiometer/Terra albedo product

Wouter Greuell,[1] Jack Kohler,[2] Friedrich Obleitner,[3] Piotr Glowacki,[4] Kjetil Melvold,[5] Erik Bernsen,[1] and Johannes Oerlemans[1]

Received 1 March 2006; revised 30 August 2006; accepted 21 November 2006; published 7 April 2007.

[1] We estimate annual anomalies of the surface mass balance of glaciers on Svalbard for the period 2000–2005 (six years), by calculating the so-called ''satellite-derived mass balance'' (B_{sat}) from time series of satellite-derived surface albedos. The method needs no other input variables. Surface albedos are extracted from the Moderate Resolution Imaging Spectroradiometer (MODIS)/Terra albedo product. We validate the MODIS albedos by comparing them with in situ measurements on Kongsvegen, and we find a low root-mean-square error of 0.04 for higher-quality MODIS data. Confidence in the MODIS product is also provided by realistic profiles of albedo along glacier centerlines. We apply the method to 18 glaciers that are evenly distributed over the archipelago. Correlation coefficients of time series of B_{sat} and direct measurements of the annual mass balance on Kongsvegen and Hansbreen are highly significant (0.94 and 0.82, respectively). Moreover, spatial distributions of the anomalies for individual years are coherent. Disadvantages of the method are that absolute values of the mass balance cannot be determined and that the interannual variability is underestimated. The latter might be corrected by equations to be established with mass balance models.

Citation: Greuell, W., J. Kohler, F. Obleitner, P. Glowacki, K. Melvold, E. Bernsen, and J. Oerlemans (2007), Assessment of interannual variations in the surface mass balance of 18 Svalbard glaciers from the Moderate Resolution Imaging Spectroradiometer/Terra albedo product, *J. Geophys. Res.*, *112*, D07105, doi:10.1029/2006JD007245.

1. Introduction

[2] Monitoring the annual surface mass balance of glaciers and ice sheets is a major task of the glaciological community. Such measurements are used for many purposes, for example, for estimating ice volume changes and therefore the contributions of glaciers and ice sheets to sea level change, for validating surface mass balance models and for detecting temporal variations in the surface mass balance. Interannual variations also serve as an analogue for variations caused by climate changes occurring over longer timescales.

[3] The classical method for obtaining mass balance is via direct measurements with networks of stakes and snow pits. A problem with direct measurements, however, is that they are labor intensive and thereby limited in space and duration. This is certainly true for the archipelago of Svalbard (62,248 km^2), which is extensively glacierized (59% of the land area according to *Liestøl* [1993]), the glaciers and ice caps having a sea level equivalent of approximately 2 cm [*Hagen et al.*, 2003].

[4] Table 1 lists all 14 glaciers in Svalbard on which mass balance measurements have been or are still being made. General information about some of these measurements and variations in the equilibrium line altitude across Svalbard can be found in the work of *Hagen and Liestøl* [1990], *Liestøl* [1993], and *Hagen et al.* [2003].

[5] While such field measurements are invaluable, they have their limitations. On Svalbard, for example, only two time series are of long duration (as of this writing, the records of Midre Lovénbreen and Austre Brøggerbreen are 37 and 38 years long, respectively), most are short (seven series span a maximum of 10 balance years), and many have not been continued up to the present (eight series). Only five series were collected on glaciers of any considerable size ($\geq$35 km^2), with the remainder collected on very small glaciers (<10 km^2). Furthermore, the measured mass balances may not be representative for all of Svalbard since all 14 glaciers are situated in a limited part of the archipelago, namely, the western and central part of the main island of Spitsbergen. None are located in the eastern part of Spits-

[1]Institute for Marine and Atmospheric Research Utrecht, Utrecht University, Utrecht, Netherlands.
[2]Norwegian Polar Institute, Tromsø, Norway.
[3]Institute for Meteorology and Geophysics, Innsbruck University, Innsbruck, Austria.
[4]Institute of Geophysics, Polish Academy of Sciences, Warsaw, Poland.
[5]Norwegian Water Resources and Energy Directorate, Oslo, Norway.

0148-0227/07/2006JD007245$09.00

Table 1. Information About Direct Mass Balance Measurements Carried Out in Svalbard

Glacier	Location	Surface Area, km^2	Period	Reference[a]
Austre Brøggerbreen	78°54′N, 11°50′E	6.1	1967–2005	2
Bertilbreen	78°30′N, 15°50′E	5.4	1975–1985	1
Bogerbreen	78°07′N, 15°37′E	5.3	1974–1986	1
Daudbreen	78°04′N, 18°49′E	4.5	1978–1983	1
Finsterwalderbreen	77°28′N, 15°18′E	35	1950–1968	1
Fridtjovbreen	77°50′N, 15°26′E	49	1987–1991	3
Grønfjordbreen	77°54′N, 14°15′E	38	1986–1991	3
Hansbreen	77°05′N, 15°40′E	56	1989–2005	2
Irenebreen	78°39′N, 12°06′E	4.3	2002–2005	2
Kongsvegen	78°51′N, 12°30′E	102	1987–2005	2
Longyearbreen	78°10′N, 15°31′E	4.0	1977–1982	1
Midre Lovénbreen	78°53′N, 12°03′E	6.0	1968–2005	2
Vöringbreen	78°02′N, 13°58′E	2.1	1967–1988	1
Waldemarbreen	78°40′N, 12°00′E	2.7	1995–2005	2

[a]References are 1, *Hagen and Liestøl* [1990]; 2, http://www.geo.unizh.ch/wgms/; 3, *Jania and Hagen* [1996].

bergen, on Nordaustlandet, on Edgeøya or on Barentsøya (see Figure 1).

[6] This provides the motivation for estimating mass balance using remote sensing methods, provided that such estimates are of sufficient quality. The strongest point of remote sensing methods is that the mass balance can, in principle, be calculated for all glaciers. Previously, *König et al.* [2004] demonstrated that under certain conditions annual mass balances can be estimated with synthetic aperture radar (SAR) satellite data. *De Ruyter de Wildt et al.* [2002] attempted to derive annual mass balances from late-summer snow lines using visible imagery, but found that this method suffered from a fundamental flaw. It occurs when, during summer, the snow line passes that of the end of the previous summer. In such years, the snow line separates last winter's snow from an earlier winter's snow, but these two types cannot be distinguished in visible imagery. The same problem occurs when SAR data are used.

[7] Here we explore the satellite albedo method discussed by *Greuell and Oerlemans* [2005]. The method is fairly simple. Input for our calculations are surface albedos derived from satellite data; no other input variables are needed. From the albedo, the total energy flux from the atmosphere to the glacier surface is estimated, which is then integrated over the ablation season and finally, by division through the latent heat of fusion, converted into the so-called "satellite-derived mass balance."

[8] The method has been applied before. *Greuell and Oerlemans* [2005] calculated the satellite-derived mass balance of the Kangerlussuaq-transect (K-transect; Greenland ice sheet) for 13 balance years. Their calculated mass balance explained 71% of the variance (corr. coeff. (r) = 0.84) in direct measurements of the mass balance. With a somewhat simpler version of the method, *De Ruyter de Wildt et al.* [2002] and *Calluy et al.* [2005] assessed the surface mass balance of six outlets of Vatnajökull, explaining variances in the measurements ranging between 0 (on Breidamerkurjökull, but with only five years of measurements) and 87% (r = 0.94). In all these studies, albedos were derived from advanced very high resolution radiometer (AVHRR) data.

[9] Our goal is to use the satellite albedo method to assess the surface mass balance of a representative set of glaciers and ice caps in Svalbard. We select 18 glaciers (Figure 1 and Table 2). Input data are taken from the Moderate Resolution Imaging Spectroradiometer (MODIS)/Terra albedo product. Since MODIS data are not available for the time before December 1999, when the satellite (Terra) carrying the instruments was launched, our study is limited to six mass balance years (1999/2000–2004/2005). In section 2 we will introduce the satellite albedo method and explain the reasons for its good performance. Section 3 then

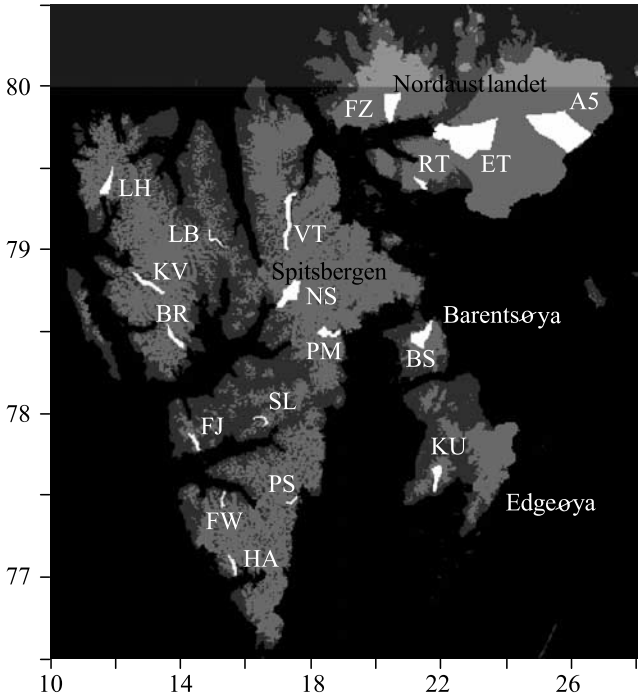

Figure 1. Map of Svalbard showing land area (dark grey), glaciated area (light grey), and the glaciers selected for this study (white), with abbreviations given in Table 2. As indicated by the brighter band at the top of the figure, the Moderate Resolution Imaging Spectroradiometer (MODIS)/Terra albedo product is not available for the area north of 80°N.

Table 2. Topographic Information and Results for the Selected Glaciers[a]

Abbreviation	Glacier	Area, km^2	Elevation Range, m	2000	2001	2002	2003	2004	2005	SD	Ice Albedo[b]
A5	Austfonna5	589	0–724	280	120	−110	−230	−20	−40	180	0.42
BS	Besselsbreen	125	47–637	260	250	−310	−410	40	170	290	0.27
BR	Borebreen	52	117–601	260	60	−20	−90	−150	−60	150	0.23
ET	Etonbreen	621	0–742	260	50	−30	10	−110	−180	150	0.44
FW	Finsterwalderbreen	20	110–649	330	120	−120	−150	−160	−10	190	—
FZ	Frazerbreen	127	9–548	290	−40	−120	−10	10	−140	150	0.44
FJ	Fridtjovbreen	32	0–495	160	30	−80	30	0	−150	110	0.24
HA	Hansbreen	32	107–512	80	−160	−20	−10	40	80	90	0.38
KV	Kongsvegen	65	125–823	450	40	−30	−10	−310	−130	250	0.33
KU	Kuhrbreen	70	14–579	540	50	−320	−340	−40	110	330	0.18
LH	Lilliehookbreen	65	74–715	180	380	−50	−70	−160	−280	240	0.37
LB	Lisbetbreen	18	122–1075	460	30	−90	30	−180	−240	250	0.13
NS	Nordenskioldbreen	142	98–1195	270	130	−90	100	−220	−180	190	0.37
PS	Perseibreen	14	81–575	740	100	−460	−650	140	130	490	0.17
PM	Petermannbreen	61	93–611	430	180	−430	−250	−50	120	310	0.27
RT	Rosenthalbreen	29	7–464	410	120	−170	−190	−20	−160	230	0.27
SL	Slakbreen	19	153–935	620	70	−250	−270	−180	10	330	0.18
VT	Veteranen	109	95–1166	510	40	−290	−50	−120	−90	270	0.27
	Mean			360	90	−160	−140	−80	−60	230	0.29

[a]The abbreviations of the first column appear in Figures 1 and 8. Area and elevation range are valid for the polygons used for our calculations and can be substantially smaller than the areas given in Table 1, which include marginal strips, tributaries, etc. Elevations were obtained from a digital elevation model produced by the Norwegian Polar Institute from their 1:100,000 series of maps. Results comprise derived annual mass balance anomalies (in millimeter water equivalent) for individual years (2000–2005), standard deviations (SD) of the mass balance anomalies (in millimeter water equivalent), and "ice albedos" (defined in section 4).

[b]For Finsterwalderbreen the shape of the profiles did not allow the determination of the "ice albedo."

describes the data, and section 4 gives the results for the selected glaciers. In section 5 we will draw conclusions and discuss relevant issues.

2. The "Satellite Albedo Method"

[10] The method we use to calculate the satellite-derived mass balance (B_{sat}) from the satellite-derived albedo (α_{sat}) is described in detail by *Greuell and Oerlemans* [2005]. Here we outline the method. The first step is the calculation of the average of the satellite-derived albedo over the glacier surface ($\overline{\alpha_{sat}}$). Thereafter, the following equation is used:

$$B_{sat} = \frac{\int_{j_1}^{j_2} \max\{I_0 \tau_{\mathrm{atm}}(1 - \overline{\alpha_{sat}}) + Q_0, 0\} dt}{L_f}, \qquad (1)$$

representing the following steps:

[11] 1. Computation of the daily mean net short-wave radiative flux at the surface by multiplying $(1 - \overline{\alpha_{sat}})$ with the daily mean incoming radiation at the top of the atmosphere (I_0) and the transmissivity of the atmosphere (τ_{atm}). The flux I_0 can be calculated very accurately with standard equations [*Garnier and Ohmura*, 1968].

[12] 2. Computation of the total energy exchange between atmosphere and glacier surface by adding a parameter (Q_0) representing the sum of the net long-wave radiative flux and the turbulent fluxes.

[13] 3. Calculation of the energy available for melt by limiting the calculations to those days for which the total energy flux is positive (toward the glacier). This is achieved by taking the maximum of the total energy flux and zero.

[14] 4. Calculation of the total melt energy for the entire ablation season by integrating between days j_1 and j_2 with a time step of one day.

[15] 5. Conversion of melt energy into amount of melt by division by the latent heat of fusion ($L_f = 0.334 \cdot 10^6$ J kg^{-1}).

[16] In summary, with the satellite albedo method we estimate interannual variations in the total amount of melt from time series of the satellite-derived albedo. Figure 2 illustrates the computation described above.

[17] The parameters τ_{atm}, Q_0, j_1 and j_2 are not determined by optimizing the fit between measured and satellite-derived mass balance. Instead, they are derived from independent data collected by weather stations. We set $\tau_{\mathrm{atm}} = 0.50$, $Q_0 = -20$ W/m^2, $j_1 = 16$ June and $j_2 = 28$ August, in accordance with measurements collected during the summer of 2003 at two weather stations on Kongsvegen (Figure 1; S1 at 180 m above sea level (asl) and S6 at 543 m asl). The value for τ_{atm} is obtained by dividing the incoming short-wave radiative flux measured at the surface by I_0. The flux Q_0 is derived from the in situ measurements of the long-wave radiative fluxes, and of temperature, wind speed and humidity. The two dates confine the period with significant melt, that is, the period for which equation (1) is valid. The values of τ_{atm} and Q_0 are averages for that period. By assigning constant values to τ_{atm}, Q_0, j_1 and j_2, we assume that the influence of the atmosphere (primarily clouds) on the incoming short-wave radiation, that the sum of the long-wave and turbulent fluxes, and that the length of the ablation season are all invariant from year to year and from glacier to glacier. Note that while these four parameters are held constant from year to year, their values affect the interannual variations in the mass balance indirectly. They determine on which days there is energy available for melt, as well as the magnitude of that energy, and thereby have an effect on the relative contribution to melt of each individual day during the summer season.

[18] Despite this assumption, the method has proven to be relatively successful [*Greuell and Oerlemans*, 2005]. There

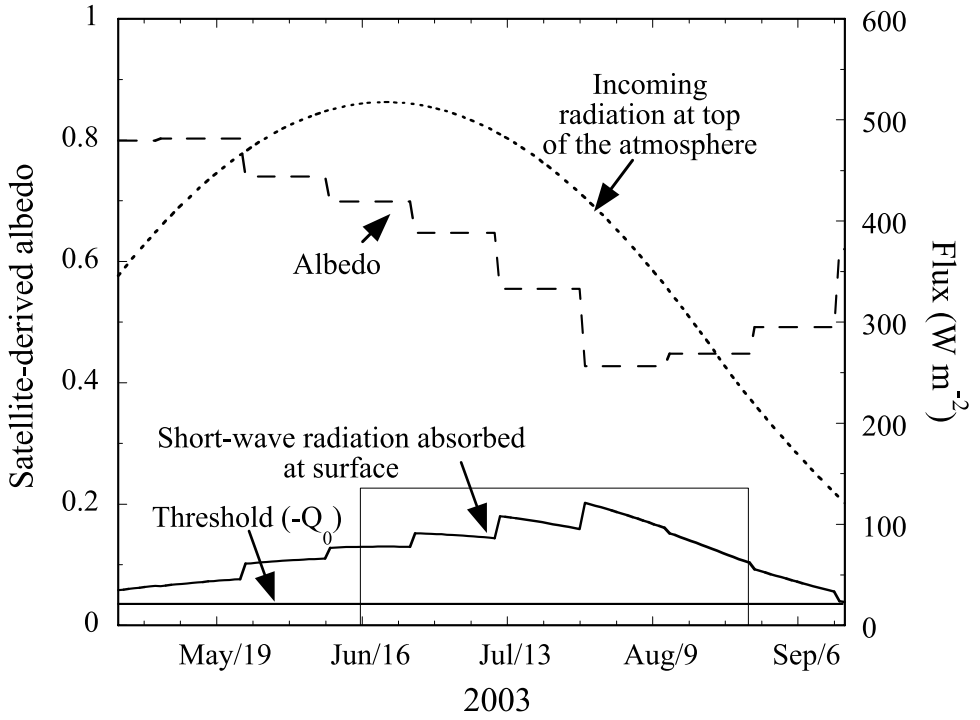

Figure 2. Illustration of the computation of B_{sat} for a single year and glacier (in this case, Kongsvegen in 2003). The input (surface albedo) is only available as a mean for periods of 16 days. It therefore changes stepwise at 16-day intervals. The same is then true for the short-wave radiation absorbed at the surface. The total melt energy is equal to the area between the curve of the absorbed short-wave radiation and the threshold within the gray box, of which the lateral sides correspond to the beginning and the end of the period for which there is significant melt. When the absorbed radiation is lower than the threshold (which does not occur in this particular graph), the area is not taken into account.

are, in theory, three reasons for the success of the method. First, net short-wave radiative flux generally constitutes the largest energy flux toward the surface during the ablation season [e.g., *Ambach*, 1979; *Hock and Holmgren*, 1996; *Greuell and Smeets*, 2001]. By assessing the interannual variation in the net short-wave radiative flux, we are therefore accounting for the most important cause of interannual variations in melt. Second, there is another link between albedo and melt captured by the method, namely the fact that increased melt rates cause a lowering of the albedo via a number of processes [see *Greuell and Oerlemans*, 2005]. This implies that there is a positive feedback between our input variable, albedo, and our output variable, which enhances any initial perturbation. Note that such perturbations are caused by perturbations in "external variables" such as atmospheric temperature and precipitation. For example, higher temperatures lead to more melt, which leads to a lower albedo, etc. On the basis of these arguments we expect that B_{sat} expresses much of the variability in the summer balance.

[19] The third reason for the success of the method is the influence of the winter balance on the albedo [*Greuell and Oerlemans*, 2005]. Less accumulation in winter results in a lower time-averaged albedo in summer since the transition from snow (higher albedo) to ice (lower albedo) occurs earlier in the season. This effect should result in a positive correlation between the winter balance and B_{sat}. Note that for the same reason there should be a positive correlation between the winter balance and the balance of the subsequent summer. We tested the latter expectation using the four longest ($\geq$16 years) mass balance time series from Svalbard (see Table 1), but none shows a significant positive correlation between the winter balance and the balance of the subsequent summer. We therefore expect only a small fraction of the variability in the winter balance to be expressed in B_{sat}.

[20] To summarize, we expect most of the variability in B_{sat} to be associated with variations in the summer balance and a lesser part with variations in the winter balance. In this paper we compare B_{sat} to measurements of both the summer and the annual mass balance.

[21] On the basis of sensitivity tests, *Greuell and Oerlemans* [2005] determined the potential and the limitations of the method for their case (the K-transect). Owing to the sensitivity of the method to the values chosen for the parameters τ_{atm} and Q_0, absolute values of the calculated mass balances appeared to be unreliable. On Svalbard, this is even more the case since accumulation and internal accumulation by refreezing of meltwater are not explicitly considered in equation (1), and both processes contribute significantly to the mass balance of glaciers in Svalbard [*Obleitner and Lehning*, 2004]. Note that equation (1) also neglects sublimation but this is not problematic as the contribution of sublimation to the mass balance is generally negligible in the Arctic [see, e.g., *Ambach*, 1979; *Hock and Holmgren*, 1996].

[22] While the method does not yield absolute values of the mass balance, *Greuell and Oerlemans* [2005] do find that it produces reasonable estimates of the interannual variability of the mass balance and that the explained variance is significant. Therefore computed anomalies of B_{sat} should provide suitable estimates of the true anomalies of the summer and/or the annual mass balance.

3. MODIS/Terra Albedo Product

[23] The main input data for this study are distilled from the MODIS/Terra albedo product. Terra is one of the two satellites bearing MODIS sensors. MODIS sensors acquire data in 36 narrow bands, of which 20 are positioned in the short-wave part of the spectrum (<3 μm). The data have a nadir resolution of 250 m (bands 1 and 2), 500 m (bands 3–7), or 1000 m (the other bands), but the resolution decreases with increasing satellite zenith angle (maximum is 55°). Since Terra is polar-orbiting and since MODIS has a wide swath (2330 km), a large number of images ($\sim$9) cover locations on Svalbard each day. The MODIS sensors are calibrated by means of a few on-board devices, leading to an absolute accuracy of the measured radiances $\leq$2% [*Justice et al.*, 2002]. On the basis of the measurements in the various narrow bands, higher-level products are produced by the MODIS Adaptive Processing System (MODAPS). Among these products is the one that we use, namely, the MODIS/Terra albedo product (MOD43B3), which can be acquired without cost from the Earth Observing System (EOS) Data Gateway.

[24] Thorough descriptions of the MODIS albedo product can be found in the work of *Schaaf et al.* [2002] and *Stroeve et al.* [2005]. Here we briefly describe the six main processing steps:

[25] 1. Calculation of the surface reflectance [see *Vermote et al.*, 2002] from the calibrated radiances at the top of the atmosphere (level 1B data). In other words, the atmospheric correction is made. For Svalbard, the algorithms use information about aerosols from climatology, about water vapor from the near-infrared MODIS bands 18 and 19 and about ozone from ancillary data (E. Vermote, personal communication, 2005). Note that "reflectance" and "radiance" here both refer to radiation in the direction of the satellite sensor.

[26] 2. Selection of surface reflectance data for clear skies with the help of the MODIS cloud mask produced by MODAPS.

[27] 3. Binning of all cloud-cleared surface reflectances into 16-day periods, which have the same starting days (Julian days 1, 17, 33, etc.) and end days each year. Data for snow-covered and snow-free surfaces are binned separately.

[28] 4. Fitting functions that describe the directional distribution of the reflected radiation (bidirectional reflectance distribution functions, BRDFs) to the data contained in each 16-day bin. MODAPS assumes BRDFs to have the following form:

$$R(\theta_s, \theta_v, \phi) = f_{iso} + f_{vol}K_{vol}(\theta_s, \theta_v, \phi) + f_{geo}K_{geo}(\theta_s, \theta_v, \phi), \quad (2)$$

where R is the reflectance, which is a function of the sun-target-satellite geometry given by the solar zenith angle (θ_s), the satellite zenith angle (θ_v) and the azimuth angle relative to the direction of the sun (ϕ). The equation prescribes R as the sum of three terms. The first term represents isotropic reflection, and the two other terms are based on the kernels K, which are prescribed functions of the sun-target-satellite geometry. The kernels used by MODAPS were specifically designed for vegetation ("vol" indicates volume scattering and "geo" geometric scattering [see *Roujean et al.*, 1992]); to our knowledge their suitability for the description of reflection by snow and ice has not been tested. The coefficients f_{iso}, f_{vol}, and f_{geo} are found by fitting equation (2) to the cloud-cleared surface reflectance data. This is done to the snow-covered data when these outnumber the snow-free data, or to the snow-free data when these outnumber the snow-covered data. A backup algorithm is employed if the coefficients in equation (2) cannot be retrieved with sufficient accuracy [*Stroeve et al.*, 2005].

[29] 5. Calculation of the black-sky albedo and the white-sky albedo by integrating equation (2) over the hemisphere. The black-sky albedo is the albedo when the incoming radiation does not have a diffuse component, and is a function of the solar zenith angle. The MODIS product gives the black-sky albedo for local solar noon. The white-sky albedo is the albedo when the incoming radiation is isotropic. Note that all processing steps 1–5 are performed on the level of the MODIS narrow bands and more specifically in bands 1–7 only.

[30] 6. Conversion of the narrowband albedos into the broadband albedo (0.3–5.0 μm) with the equations of *Stroeve et al.* [2005]. These are implemented for predominantly snow scenes as determined with a Normalized Difference Snow Index (NDSI) threshold (C. Schaaf, personal communication, 2005). For other scenes the conversion is done with the equations of *Liang et al.* [1999].

[31] By taking all data from a 16-day period together for the calculation of a single albedo valid for the whole period, it is assumed that the surface characteristics do not change during that period. This can be a poor assumption for glaciers, especially in summer. We speculate that the associated errors can be considerable when daily values of the albedos are needed. This study is concerned with obtaining summer mean values, however, so the 16-day averaging should not be a problem.

[32] The earlier studies of *De Ruyter de Wildt et al.* [2002], *Calluy et al.* [2005], and *Greuell and Oerlemans* [2005] all use AVHRR data as input. AVHRR data have the advantage that they go back in time to 1979, whereas summer time MODIS data are only available from the year 2000 onward. Nevertheless, we have chosen to use MODIS data for several reasons. The first advantage of the MODIS data is the high absolute accuracy of the radiances measured by the sensors ($\leq$2%). As *Greuell and Oerlemans* [2005] discuss, the accuracy of the calibration coefficients of the AVHRR sensors is much poorer ($\sim$10%), which causes undesired interannual variation in B_{sat} during the mentioned studies. Another advantage of MODIS is the availability of the MODIS surface albedo product, which is based on all the satellite data covering the location in question, while higher-level products of AVHRR data exist only for special cases. In addition, while the resolution of the albedo product (1 km) is similar to the nadir resolution of AVHRR data (1.1 km), it is much better than the resolution of AVHRR data (2.4*6.9 km) acquired at the largest view zenith angle (55.4°). Finally, MODIS data can be acquired without costs.

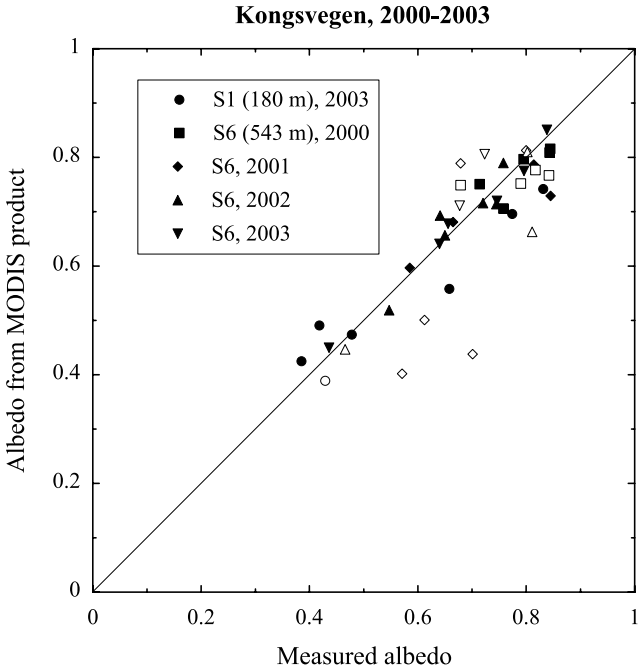

Figure 3. Comparison of surface albedos distracted from the MODIS/Terra albedo product with in situ measurements from two sites on Kongsvegen. Solid symbols correspond to higher-quality data.

[33] We validate the albedo product by comparing it with in situ measurements obtained at two sites on Kongsvegen. At site S1 (180 m asl), located in the ablation area near the terminus of the glacier, data are available for one summer. At S6 (543 m asl), located near the elevation of the mean equilibrium line, there are four summers of data. Measurements were made with a Kipp & Zonen CNR1 sensor at S1 (spectral band: 0.305–2.8 μm) and with a Kipp & Zonen CNR1 sensor and a Swissteco SW2 sensor at S6. The downward looking instruments viewed an area of roughly 10 by 10 m. From the recorded hourly means of short-wave incoming and outgoing radiation, we selected the values for the hour around local solar noon and computed the albedo. We averaged these daily albedos over the same 16-day periods as the MODIS product. The result was compared with the black-sky MODIS albedos for the pixel nearest to the location of the ground measurement.

[34] Figure 3 shows all the available points for comparison. Some of these points correspond to 16-day periods for which the mean solar zenith angle was very low (before 9 May and from 13 August onward) or to 16-day periods when a large fraction of the raw MODIS data (6–11 days), on which the albedo product is based, was not available at all. These two categories of points are considered as lower-quality data and are represented by open symbols in the graph. Clearly, the lower-quality MODIS data show a much poorer agreement with the measurements (root-mean-square error (RMSE) = 0.11) than do the remaining, higher-quality MODIS data (RMSE = 0.04). This last value is identical to the performance of MODIS albedo product "highest-quality data" selected by and compared to in situ measurements from the Greenland ice sheet by *Stroeve et al.* [2005]. On average, our higher-quality MODIS albedos are slightly lower (−0.01) than the measurements. In agreement with *Stroeve et al.* [2005], this negative bias tends to increase with albedo.

[35] Causes of the differences between the MODIS product and the in situ measurements can be manifold. The in situ measurements mainly suffer from the fact that most of the time the unattended instrumentation is not parallel to the underlying surface. Errors in the MODIS product are introduced during every processing step. However, even if all those processing steps were performed without error, the MODIS albedos would be in error because no correction for surface tilt is made. Slope-induced errors will be small, though, since the slopes at the location of the ground measurements are small (1.8° toward NNW at S1 and 1.1° toward NW at S6). Errors in the MODIS product are also caused by uneven sampling in time due to clouds and by the fact that the MODIS albedo product is based on clear-sky data only, whereas the in situ data are obtained under both cloudy and clear conditions. This is important because clouds affect the spectrum of the incoming short-wave radiation and therefore the albedo [*Key et al.*, 2001]. Finally, inhomogeneity of the terrain causes differences between the MODIS and the in situ albedos. Whereas MODIS pixels cover an area of 1 by 1 km, the ground-based instruments view an area of roughly 10 by 10 m. Perhaps inhomogeneity of the terrain caused the relatively large bias of the albedos for S1. Given all these possible causes of differences between calculated and measured albedo, a bias of 0.01 and an RMSE of 0.04 are remarkably small.

[36] The comparison of the MODIS product with in situ measurements provides confidence in the product. Confidence is strengthened by an analysis of black-sky albedo variations along the centerlines of the selected glaciers, which generally appear realistic. Figure 4 shows as an example the 2003 profiles of Kongsvegen, which exhibit the common, expected evolution (Figure 4a), and of Besselsbreen [*Dowdeswell and Bamber*, 1995], which exhibits an uncommon evolution (Figure 4b).

[37] For Kongsvegen the first profile in May 2003 shows high albedos ranging between 0.70 and 0.85. During the summer season the albedo decreases continuously at all elevations. The rate of change has a maximum roughly between 300 and 450 m asl (between distances of 7 and 14 km from the terminus). The snow line is not sharp but gradually and clearly migrates upward along the glacier. The two profiles for August 2003 are almost identical and show snow lines at elevations of 555 and 590 m asl, an elevation comparable to the observed equilibrium line altitude of 608 m asl. In August, the mean albedos for the lowest 15 km of the glacier, which is bare ice, are 0.34 (5 August) and 0.39 (17 August).

[38] During the first part of the summer 2003, the evolution of the albedo profiles for Besselsbreen is qualitatively similar to the evolution of the profiles for Kongsvegen. However, then an abnormal change occurs. Between 4 July and 5 August, the albedo decreases by ~0.30 in the higher half of the glacier and by only ~0.15 in the lower half of the glacier, so the two albedo profiles of August become "inversed"; that is, albedo decreases with elevation. The profile of 5 August has an albedo of 0.31 in the lower half of the glacier and 0.24 in the upper half of the glacier. These values are clearly indicative of ice, which

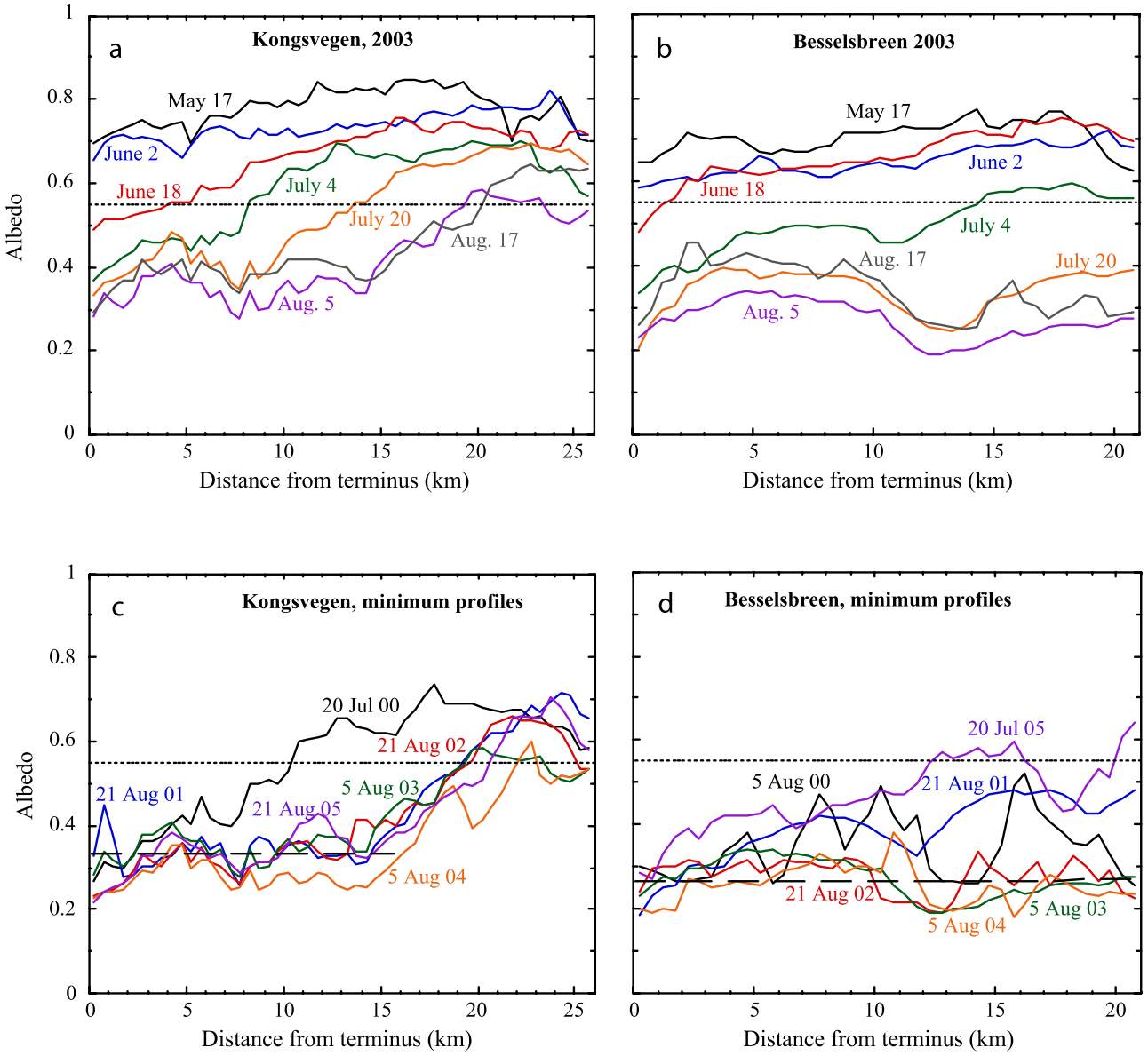

Figure 4. Surface albedo along the centerlines of Kongsvegen and Besselsbreen according to the MODIS/Terra albedo product, showing (a, b) summer of 2003 and (c, d) "minimum albedo profiles" for all six summers. Curves are labeled with the dates in the middle of the 16-day periods they represent. Lines with short dashes designate the threshold albedo for the separation of snow from ice (0.55). The intersection of a profile with this line gives the position of the snow line. We define the "minimum albedo profile" as the length profile with the lowest average albedo among all profiles for a particular year. Lines with long dashes give the "ice albedos" of Kongsvegen and Besselsbreen as estimated from the graphs. These values of the "ice albedo" are used for further analysis in section 4.

apparently became exposed up to the highest elevation of Besselsbreen (616 m asl). We do not know what the cause of these uncommon albedo profiles is, but do not have any reason to believe it to be an artifact of the retrieval. Minimum albedo profiles for 2002 and 2004 are similar to the minimum albedo profile for 2003 (Figure 4d).

[39] For Kongsvegen minimum albedo profiles (Figure 4c) are almost identical for four out of the six years. The two outliers are much higher minimum albedos for 2000 and somewhat lower minimum albedos for 2004, the years of maximum and minimum annual surface mass balance (see section 4).

4. Results

[40] For this study we select 18 glaciers more or less evenly distributed over the archipelago of Svalbard (Figure 1). Glaciers north of 80°N are excluded since MODIS albedo products are not available above this latitude. None of the selected glaciers has a surface area smaller than 14 km^2, so that all glaciers are covered by a sufficient amount of

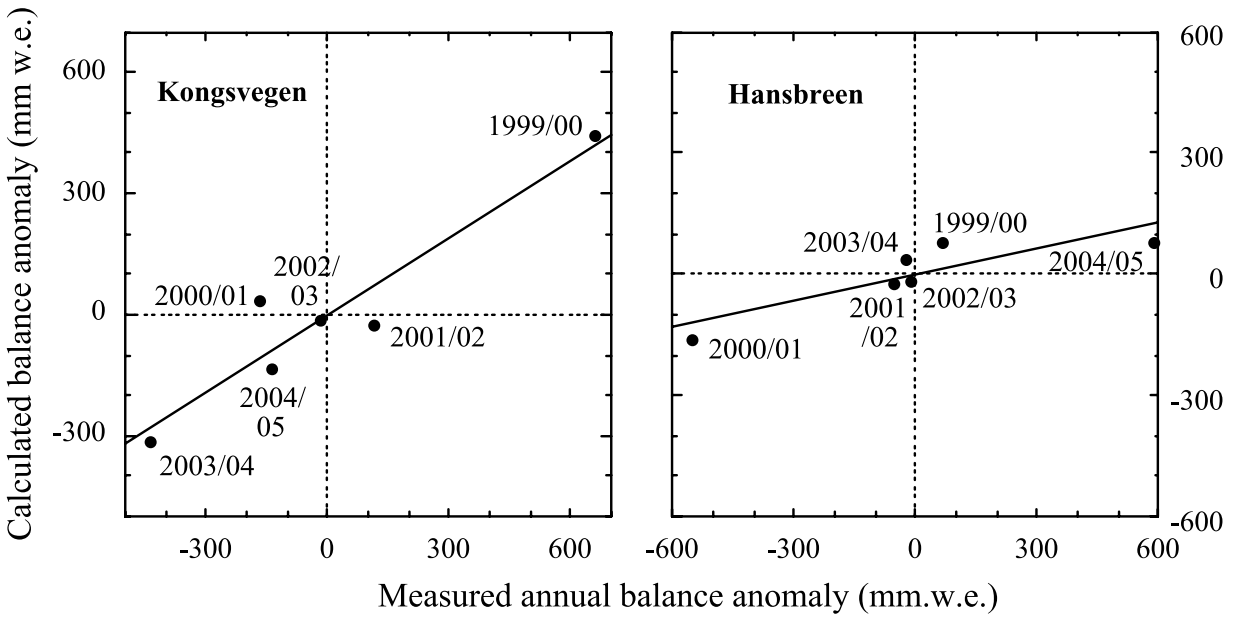

Figure 5. Comparison of the anomalies in B_{sat} with direct measurements of the annual balance. Scales on the vertical and horizontal axes and in both panels are the same. The lines indicate least squares fits.

MODIS pixels. In view of possible future modeling work, we prefer nonsurging glaciers. Twelve of the selected glaciers have indeed not been observed to surge [*Liestøl*, 1993; J. O. Hagen, personal communication, 2005]; the other six glaciers have surged but are chosen because they have been the subject of some glaciological research. Among the selected glaciers are three drainage basins belonging to the ice caps of Austfonna and Vestfonna on Nordaustlandet, as delineated by *Dowdeswell* [1986].

[41] Using the 1:250,000 Norwegian Polar Institute maps, we delimit the area of calculation for each glacier with a polygon covering the entire glacier surface, masking out the edge with a narrow (0–500 m) marginal strip.

[42] We then calculate the mean black-sky albedo for all pixels within each polygon and within an elevational range around the midelevation of the glacier. More precisely, we exclude all pixels located within the lowest 25% and the highest 25% of the total elevation range of the glacier. This left us with between 42% (Petermannbreen) and 91% (Slakbreen) of all pixels within the polygons. Elevations were taken from a Digital Elevation Model produced by the Norwegian Polar Institute from their 1:100,000 series of maps. The maps are derived from aerial photographs of different ages, with some of the earliest maps dating back to 1936.

[43] We truncate the range of elevations because this is suggested by comparison of B_{sat} with direct measurements at individual sites along the K-transect [*Greuell and Oerlemans*, 2005]. On the lowest parts of glaciers, ice is exposed during the largest part of most summers; similarly, the highest parts of glaciers are snow-covered during the largest part of most summers. Therefore interannual variations in albedo and B_{sat} are relatively small at the lowest and highest elevations, where consequently the correlation between B_{sat} and the measurements is relatively low. The method performs best at and just below the mean equilibrium line. However, since we do not know the altitude of the mean equilibrium line of the selected glaciers (this would require another retrieval method), we choose an elevational band around the midelevation of the glacier instead of around the equilibrium line. Despite restricting the elevational distribution, we assume that the calculated anomaly is nonetheless representative of the entire glacier since interannual variations in specific mass balance for different elevations are highly correlated [e.g., *Kuhn*, 1984].

[44] The anomalies presented in Figures 5–7 and Table 2 are deviations from the mean over the six available balance years 1999/2000–2004/2005. We are able to compare these values to the annual and summer balances of two glaciers, Kongsvegen and Hansbreen. Correlation coefficients of the calculated anomalies with the annual balances are 0.94 (Kongsvegen) and 0.87 (Hansbreen), which means that 89% and 75%, respectively, of the variance are explained. Correlation coefficients with the measured summer balance are 0.93 and 0.82, respectively (86% and 67% of the variance explained). All these correlation coefficients are significant at the 97.5% level, or better. These correlation coefficients are in line with those found by *De Ruyter de Wildt et al.* [2002] and *Calluy et al.* [2005] for outlets of Vatnajökull, Iceland (up to 0.94 for 5–10 years of data) and those found by *Greuell and Oerlemans* [2005] for the K-transect, Greenland (0.84 for 13 years of data). We use the standard deviation (SD) as a measure of the interannual variability. For both Kongsvegen and Hansbreen the SD in B_{sat} is lower than in the measured mass balance. For Hansbreen (an SD of 90 mm w.e. in the calculations, 360 mm w.e. in the measured annual balance and 250 mm w.e. in the measured summer balance) the underestimate is more severe than for Kongsbreen (an SD of 250 mm w.e. in the calculations and 370 mm w.e. in both the measured annual and the measured summer balance). In summary, B_{sat} correlates well with measurements of both the annual

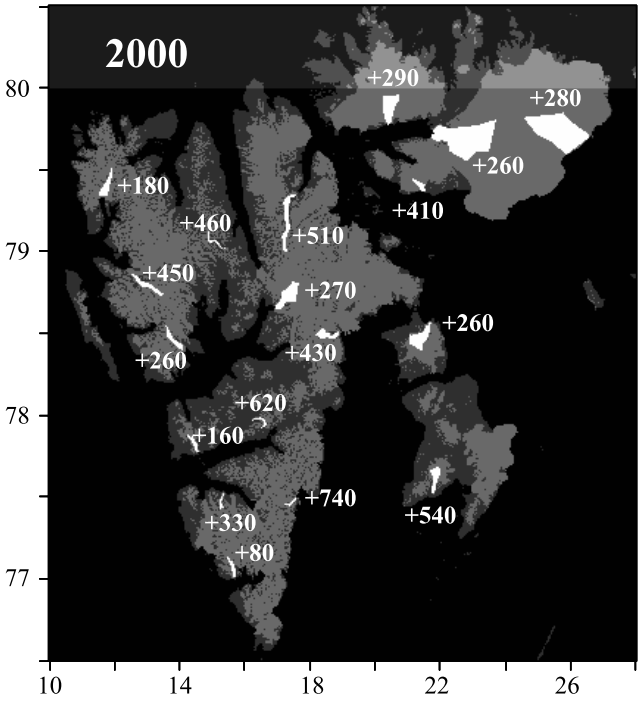

Figure 6. Anomalies in B_{sat} (mm w.e.) for the year 2000 for the 18 selected glaciers.

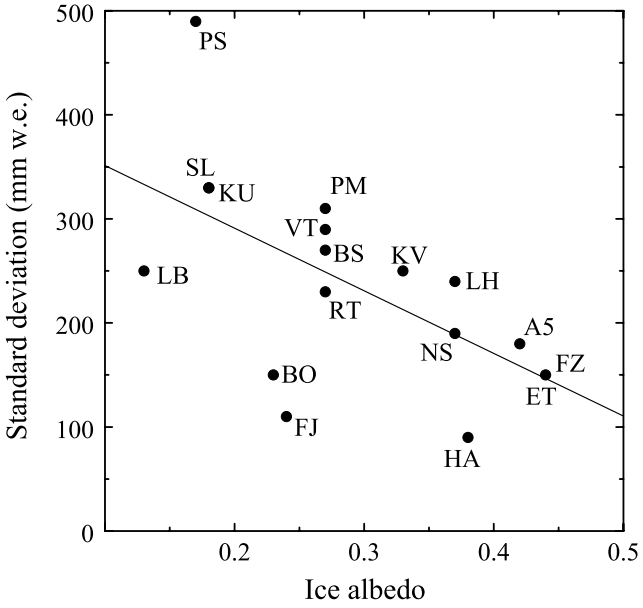

Figure 8. Standard deviation of the annual mass balance anomaly as a function of the "ice albedo" (defined in the text). Full names of the glaciers corresponding to the abbreviations are in Table 2. The lines indicate least squares fits.

and the summer mass balance but the absolute magnitude of the anomalies in B_{sat} is less than for the measurements.

[45] Since the comparison with measurements from Kongsvegen and Hansbreen provides confidence in our results, we provide the annual anomalies of B_{sat} for 2000–2005 for all the 18 selected glaciers in Table 2.

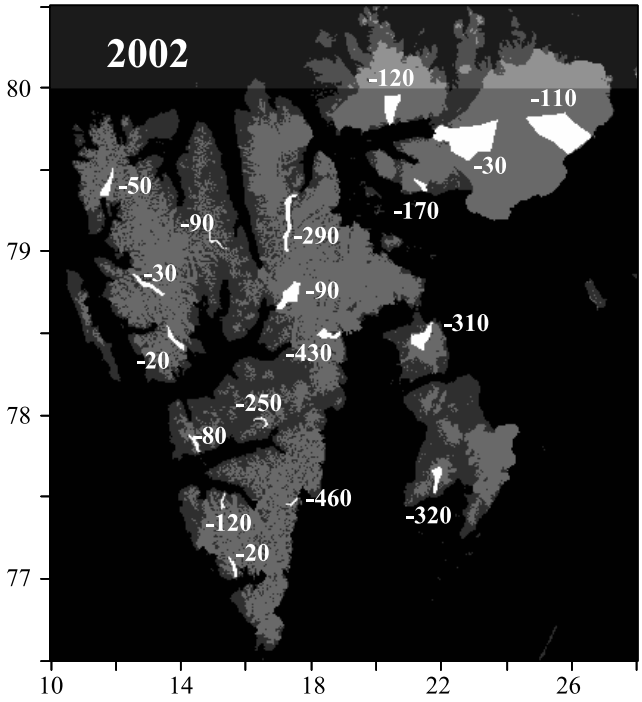

Figure 7. Anomalies in B_{sat} (millimeter water equivalent) for the year 2002 for the 18 selected glaciers.

Spatial distributions of the annual signals appear to be highly coherent. Figures 6 and 7 show the anomalies across the archipelago for the summers of 2000 and 2002, the years with the highest and the lowest mean (over the 18 glaciers) B_{sat} of all six years. Anomalies are consistently positive for all 18 glaciers in 2000 and negative for all glaciers in 2002. This coherency cannot be due to errors in the calibration coefficients of the MODIS sensors with variations on a timescale of one or several years. Errors, even absolute ones, are far too small ($\leq$2%).

[46] As a measure of the interannual variability, Table 2 also lists the SDs of anomalies for the 18 glaciers. Probably, these values underestimate the true variability, as suggested by comparison of our results with the measured mass balances of Kongsvegen and Hansbreen. We find that interannual variability in B_{sat} decreases with the "ice albedo" (Figure 8), where the "ice albedo" is defined as the mean albedo over the ice-covered part of the length profiles of glaciers, considering only the two or three lowest minimum albedo profiles (see Figures 4c and 4d). The mechanism behind this link can be understood by comparing a warm and a cold summer and the effect of the ice albedo on the difference in B_{sat} between those two summers. More melting occurs in a warm summer, leading to an earlier appearance of the ice at the surface. As long as there is ice at the surface in the warm summer and snow at the surface in the cold summer, the contrast in B_{sat} between the two summers (the interannual variability) is enhanced owing to the difference between the ice and the snow albedo. Obviously, this enhancement increases with the difference between the ice and the snow albedo. The difference is mostly a function of ice albedo, which can vary considerably from glacier to glacier, and not of the snow albedo. The latter is determined by interaction of

the snow with the atmosphere and not by the location or the setting of the glacier.

[47] Note that in Figure 8, Perseibreen (PS) is an outlier; this is most likely owing to the effect of a surge on the albedo. According to *Dowdeswell and Benham* [2003], Perseibreen surged between June 2000 and April 2002. In 2005 the surge was still continuing, at least in the sense that there was extensive crevassing.

[48] We perform a number of tests on Kongsvegen and Hansbreen to determine the sensitivity of the results to settings of the various parameters and assumptions. In each test we change only one parameter or assumption relative to the reference. We take the white-sky instead of the black-sky albedo from the MODIS product, shift j_1 from 16 June to 6 June and j_2 from 28 August to 7 September, enhance τ_{atm} from 0.50 to 0.55, increase Q_0 from -20 to -10 W/m^2 and calculate the mean albedo over the entire glacier and over an elevational range around the midelevation of 20% of the total range, instead of taking an elevational range of 50%. We performed these tests both for Kongsvegen and for Hansbreen. In all cases the correlation coefficient is changed by a maximum of ± 0.03 and the standard deviation of the annual anomalies by less than 12% for Kongsvegen and less than 19% for Hansbreen. The only exception is a decrease in the correlation coefficient by 0.05 when the entire surface of Kongsvegen is considered instead of the elevation band. So, our results are hardly sensitive to uncertainties in model parameters, with the possible exception of the choice of elevation band. The 50% elevation band is chosen for our calculations as a compromise between taking as many pixels as possible (since the goal is to calculate the mean mass balance of the entire glacier) and optimal performance of the method (the correlation coefficient decreases when the highest and the lowest part of the glaciers are included).

5. Discussion and Conclusions

[49] We estimate annual anomalies of the surface mass balance of 18 glaciers evenly distributed over the archipelago of Svalbard using a method introduced by *De Ruyter de Wildt et al.* [2002] and further developed by *Greuell and Oerlemans* [2005]. Temporal and spatial variations in satellite-derived surface albedos, in this case taken from the MODIS/Terra albedo product, are the only input for the calculations.

[50] On the basis of theoretical arguments (see section 2), B_{sat} should, in the first place, provide an estimate of the summer balance, and not of the annual balance. However, we argued then that since summer and annual balance are strongly correlated, B_{sat} should also provide a good estimate of the annual balance. Indeed, over the six years considered in this study, the time series of summer and annual balance of Kongsvegen and Hansbreen have correlations coefficients of 0.97 and 0.88, respectively. It is interesting to note that these correlation coefficients are so high because winter balances vary much less than summer balance (SDs for the period 1999/2000–2004/2005 are only 80 and 190 mm w.e. for winter balances compared to 370 and 250 mm w.e. for summer balances on Kongsvegen and Hansbreen, respectively). So, because most of the variations in the annual balance are due to variations in the summer balance, we expect a high correlation between B_{sat} and the annual balance. We argued then that, in theory, the relation between B_{sat} and the annual balance should be strengthened by a positive correlation between the winter balance and B_{sat} owing to the effect of winter accumulation on summer albedo. The same argument predicts a positive correlation between the winter balance and the balance of the subsequent summer, which, however, does not show up in the long series of mass balance measurements in Svalbard. Nevertheless, statistics inferred from a comparison of B_{sat} with the annual and summer balances from Kongsvegen and Hansbreen show slightly higher correlations for the annual balances, although the differences are not significant owing to the small number of years for which the MODIS data are available (six). In summary, we cannot conclude whether B_{sat} should be considered as a predictor of the summer or of the annual balance. Experiments with mass balance models would shed light on this issue.

[51] Confidence in our results is not only provided by the highly significant correlation coefficients between B_{sat} and direct measurements but also by the spatial coherence of the anomalies for individual years (Figures 6 and 7).

[52] On the other hand, the comparison of the direct measurements on Kongsvegen and Hansbreen indicates that our method underestimates the interannual variability in the mass balance (by 32 and 63%, respectively). *Greuell and Oerlemans* [2005] also find an underestimate of the interannual variability for the K-transect (Greenland), but it was only 7%. To obtain the correct amount of interannual variability is important as it is somehow linked to the climate sensitivity of glaciers. We suggest performing experiments with mass balance models based on the energy balance approach [*Klok and Oerlemans*, 2002; *Greuell and Genthon*, 2004] to obtain more insight into the links between interannual variations in climatic variables (like atmospheric temperature and precipitation) and B_{sat} and the mass balance. Those experiments might then lead to the establishment of an equation to be used for scaling the anomalies of B_{sat}, so that the variability in B_{sat} matches the variability in the true mass balance. Such scaling might be a function of the ice albedo, as suggested by Figure 8, and of the mean annual amount of precipitation [see *Oerlemans and Fortuin*, 1992].

[53] A disadvantage of the satellite albedo method is its inability to provide a useful estimate of the absolute value of the surface mass balance, either the annual or the summer balance. Direct measurements are needed to tie the anomalies of the satellite-derived mass balance to absolute values. Note, however, that for estimating the climate sensitivity of glaciers, interannual variations in the mass balance provide more information than absolute values of the mass balance (the mean over a period of many years).

[54] The present study provides considerable confidence in the MODIS/Terra albedo product. Validation with in situ measurements is favorable (Figure 3; root-mean-square error of the high-quality data = 0.04) and the temporal development of the length profiles of the albedo along the selected glaciers appears realistic (Figure 4). However, the MODIS product has some limitations. It is not archived for areas poleward of 80°, and the resolution (1 km) is too coarse for small glaciers. Both these limitations can, in principle, be overcome. The archive could be extended to regions beyond 80° and a resolution of 0.25 km could be

achieved because part of the input data (level 1B), namely, the data in bands 1 and 2, is available at that resolution. As *Greuell and Oerlemans* [2004] show, the information contained in these two bands is sufficient for an accurate conversion of the narrowband albedos into the broadband albedo. Another limitation of MODIS albedos, and generally of albedos derived from any type of satellite sensor, is the difficulty to obtain them for areas with a low frequency of clear skies. However, our comparison with in situ data (Figure 3) and the fact that the albedo profiles of the selected glaciers seem realistic (Figure 4) suggest that clouds do not hamper recovery of realistic albedos for Svalbard. Finally, it is a major limitation that the length of the MODIS time series is currently limited to only six years.

[55] In view of the results of the present study and previous studies for glaciers in Iceland [*De Ruyter de Wildt et al.*, 2002; *Calluy et al.*, 2005] and for the Greenland ice sheet [*Greuell and Oerlemans*, 2005], we conclude that the method employed in this study is an inexpensive and relatively simple tool that can be used to provide estimates of the annual mass balance anomalies for many glaciers in the world. Exceptions are for glaciers poleward of 80°, glaciers that are too small to be covered by a sufficient number of satellite pixels, and glaciers in areas where cloudy skies are too frequent.

[56] **Acknowledgments.** Our research was sponsored by SPICE (Space borne measurements of Arctic glaciers and implications for sea level; EU-grant EVK2-2001-00262 SPICE) and ICEMASS (EU-grant-ENV4-CT97-0490).

References

Ambach, W. (1979), Zum Wärmehaushalt des Grönländischen Inlandeises: Vergleichende Studie im Akkumulations- und Ablationsgebiet, *Polarforschung*, *49*(1), 44–54.

Calluy, G. H. K., H. Björnsson, J. W. Greuell, and J. Oerlemans (2005), Estimating the mass balance of Vatnajökull from NOAA-AVHRR imagery, *Ann. Glaciol.*, *42*, 118–124.

De Ruyter de Wildt, M. S., J. Oerlemans, and H. Björnsson (2002), A method for monitoring glacier mass balance using satellite albedo measurements: Application to Vatnajökull (Iceland), *J. Glaciol.*, *48*(161), 267–278.

Dowdeswell, J. A. (1986), Drainage-basin characteristics of Nordaustlandet ice caps, Svalbard, *J. Glaciol.*, *32*(110), 31–38.

Dowdeswell, J. A., and J. L. Bamber (1995), On the glaciology of Edgeøya and Barentsøya, Svalbard, *Polar Res.*, *14*(2), 105–122.

Dowdeswell, J. A., and T. J. Benham (2003), A surge of Perseibreen, Svalbard, examined using aerial photographs and ASTER high-resolution satellite imagery, *Polar Res.*, *22*, 373–383.

Garnier, B., and A. Ohmura (1968), A method of calculating the direct short-wave radiation income on slopes, *J. Appl. Meteorol.*, *7*, 796–800.

Greuell, W., and C. Genthon (2004), Modelling land-ice surface mass balance, in *Mass Balance of the Cryosphere: Observations and Modelling of Contemporary and Future Changes*, edited by J. L. Bamber and A. J. Payne, pp. 117–168, Cambridge Univ. Press, New York.

Greuell, W., and J. Oerlemans (2004), Narrowband-to-broadband albedo conversion for glacier ice and snow: Equations based on modeling and ranges of validity of the equations, *Remote Sens. Environ.*, *89*, 95–105.

Greuell, W., and J. Oerlemans (2005), Assessment of the surface mass balance along the K-transect (Greenland ice sheet) from satellite-derived albedos, *Ann. Glaciol.*, *42*, 107–117.

Greuell, W., and C. J. J. P. Smeets (2001), Variations with elevation in the surface energy balance on the Pasterze (Austria), *J. Geophys. Res.*, *106*(D23), 31,717–31,727.

Hagen, J. O., and O. Liestøl (1990), Long-term glacier mass-balance investigations in Svalbard, 1950–88, *Ann. Glaciol.*, *14*, 102–106.

Hagen, J. O., K. Melvold, F. Pinglot, and J. A. Dowdeswell (2003), On the net mass balance of the glaciers and ice caps in Svalbard, Norwegian Arctic, *Arct. Antarct. Alp. Res.*, *35*(2), 264–270.

Hock, R., and B. Holmgren (1996), Some aspects of energy balance and ablation of Storglaciären, northern Sweden, *Geogr. Ann.*, *78A*(2–3), 121–132.

Jania, J., and J. O. Hagen (Eds.) (1996), *Mass Balance of Arctic Glaciers*, *Rep. 5*, 62 pp., Int. Arctic Sci. Comm., Stockholm.

Justice, C. O., J. R. G. Townshend, E. F. Vermote, E. Masuoka, R. E. Wolfe, N. Saleous, D. P. Roy, and J. T. Morisette (2002), An overview of MODIS land data processing and product status, *Remote Sens. Environ.*, *83*(1), 3–15.

Key, J. R., X. Wang, J. C. Stroeve, and C. Fowler (2001), Estimating the cloudy-sky albedo of sea ice and snow from space, *J. Geophys. Res.*, *106*(D12), 12,489–12,497.

Klok, E. J., and J. Oerlemans (2002), Model study of the spatial distribution of the energy and mass balance of Morteratschgletscher, Switzerland, *J. Glaciol.*, *48*(163), 505–518.

König, M., J.-G. Winther, J. Kohler, and F. König (2004), Two methods for firn-area and mass-balance monitoring of Svalbard glaciers with SAR satellite images, *J. Glaciol.*, *50*(168), 116–128.

Kuhn, M. (1984), Mass budget imbalances as criterion for a climatic classification of glaciers, *Geogr. Ann.*, *66A*(3), 229–238.

Liang, S., A. H. Strahler, and C. W. Walthall (1999), Retrieval of land surface albedo from satellite observations: A simulation study, *J. Appl. Meteorol.*, *38*, 712–725.

Liestøl, O. (1993), Glaciers of Svalbard, Norway, in *Satellite Image Atlas of Glaciers of the World, Europe*, edited by R. S. Williams and J. G. Ferrigno, *U. S. Geol. Surv. Prof. Pap.*, *1386-E*, 164 pp.

Obleitner, F., and M. Lehning (2004), Measurement and simulation of snow and superimposed ice at the Kongsvegen glacier, Svalbard (Spitzbergen), *J. Geophys. Res.*, *109*, D04106, doi:10.1029/2003JD003945.

Oerlemans, J., and J. P. F. Fortuin (1992), Sensitivity of glaciers and small ice caps to greenhouse warming, *Science*, *258*, 115–117.

Roujean, J.-L., M. Leroy, and P.-Y. Deschamps (1992), A bidirectional reflectance model of the Earth's surface for the correction of remote sensing data, *J. Geophys. Res.*, *97*(D18), 20,455–20,468.

Schaaf, C. B., et al. (2002), First operational BRDF, albedo and nadir reflectance products from MODIS, *Remote Sens. Environ.*, *83*, 135–148.

Stroeve, J., J. E. Box, F. Gao, S. Liang, A. Nolin, and C. Schaaf (2005), Accuracy assessment of the MODIS 16-day albedo product for snow: Comparisons with Greenland in situ measurements, *Remote Sens. Environ.*, *94*, 46–60.

Vermote, E. F., N. Z. El Saleous, and C. O. Justice (2002), Atmospheric correction of MODIS data in the visible and middle infrared: First results, *Remote Sens. Environ.*, *83*, 97–111.

E. Bernsen, W. Greuell, and J. Oerlemans, Institute for Marine and Atmospheric Research Utrecht, Utrecht University, Princetonplein 5, NL-3584 CC Utrecht, Netherlands. (w.greuell@hetnet.nl)

P. Glowacki, Institute of Geophysics, Polish Academy of Sciences, 01-452 Warsaw, Poland.

J. Kohler, Norwegian Polar Institute, N-9296 Tromsø, Norway.

K. Melvold, Norwegian Water Resources and Energy Directorate, N-0301 Oslo, Norway.

F. Obleitner, Institute for Meteorology and Geophysics, Innsbruck University, A-6020 Innsbruck, Austria.